World Journal of Advanced Research and Reviews
eISSN: 2581-9615 CODEN (USA): WJARAI
Cross Ref DOI: 10.30574/wjarr
Journal homepage: https://wjarr.com/

(RESEARCH ARTICLE)

Check for updates

Structural, electronic, mechanical, thermodynamic and optical properties of $RaHfO_3$ crystal scrutinized by density functional theory

Md. Rajib Munshi [1,*], Md Al Masud [2], Mita Chakraborty [1], Md. Zakir Hossain [3], Nakib Al Kauser [4], Rakibul Islam [5] and Md. Rubel Shaikh [6]

[1] *Department of Physics, European University of Bangladesh, Dhaka-1216, Bangladesh.*
[2] *Department of IPE, European University of Bangladesh, Dhaka-1216, Bangladesh.*
[3] *Department of Civil Engineering, European University of Bangladesh, Dhaka-1216, Bangladesh.*
[4] *Department of planning and development, European University of Bangladesh, Dhaka-1216, Bangladesh.*
[5] *Department of Controller of Examination, European University of Bangladesh, Dhaka-1216, Bangladesh.*
[6] *Department of ICT, European University of Bangladesh, Dhaka-1216, Bangladesh.*

World Journal of Advanced Research and Reviews, 2025, 25(02), 2140-2149

Publication history: Received on 05 January 2025; revised on 22 February 2025; accepted on 25 February 2025

Article DOI: https://doi.org/10.30574/wjarr.2025.25.2.0513

Abstract

In this present study, electronic, mechanical, thermodynamic and optical properties of $RaHfO_3$ crystal were investigated by Generalized Gradient Approximation (GGA) based on PBE, RPBE, and PBEsol and hybrid B3LYP methods. The calculated bandgap energies (Eg) of $RaHfO_3$ were found to be 2.247 eV, 2.178 eV, 2.095 eV, and 3.520 eV, as determined using the PBE, RPBE, PBEsol, and B3LYP approaches, respectively. The atomic orbital properties of Ra, Hf, and O in $RaHfO_3$ were analyzed through total and partial density of states (DOS) analysis. Mulliken population charge analysis provided insights into the bonding characteristics of the $RaHfO_3$ crystal. Mechanical stability was verified using the Born stability criterion, and Poisson's ratio and Pugh's ratio were evaluated to assess ductile strength and elastic anisotropy. To find out the material's thermodynamic stability and state behavior, thermophysical factors were seized at. The $RaHfO_3$ crystal demonstrates both mechanical and thermal stability, along with ductile behavior and elastic anisotropy. Its optical properties were thoroughly evaluated focusing on energy and wavelength, both approaches confirmed that $RaHfO_3$ exhibits remarkable absorption in the visible and ultraviolet regions. These outstanding properties suggest that $RaHfO_3$ could be a promising candidate for photocatalytic applications, demonstrating efficient responsiveness to visible light.

Keywords: Electronic Structure; DOS; PDOS; Mechanical; Thermodynamic; Optical Properties

1. Introduction

For producing electricity, providing heat, and powering transportation systems natural gas, fuel, and biofuels, are primarily used [1-2]. However, their continued use depletes valuable resources and poses significant environmental challenges. In response to this challenge, scholars are diligently investigating alternative energy sources and pushing the boundaries of material science to uncover novel materials and improve the characteristics of those already in existence today [3-5]. This ongoing research is essential for developing sustainable solutions to meet the growing global energy demand. The ABO_3 formula is widely used to characterize oxide-perovskites, where "A" represents alkaline earth metals such as Ca, Sr, Ra and "B" denotes transition metals like Ti, Mn, Fe, Co etc and "O" represents the oxide ion. Perovskite materials are cost-effective and exhibit excellent compatibility with existing economic infrastructures [6-7]. Recent advancements in computational techniques have enabled the evaluation of a wide array of material properties, encompassing electronic, magnetic, and mechanical attributes. The results from these computational approaches show

* Corresponding author: Md. Rajib Munshi.

strong correlation with experimental data, validating their accuracy [8]. Additionally, these materials often feature large surface areas and enhanced photocatalytic activity, which has been extensively investigated in theoretical studies of various semiconductors, including $SrHfO_3$, $BaHfO_3$ and $CaHfO_3$ etc [9-11]. There is considerable curiosity surrounding the application of Hf and its derivatives; however, $RaHfO_3$ has not garnered significant focus in this area. Prior to the technological application of $RaHfO_3$, a thorough scientific review is essential [12]. Moreover, first-principles computation is an extremely successful way for undertaking theoretical studies of these features [13-14]. Scientists have thus far paid little attention to the physical properties of RaHfO3. In an attempt to fill this information vacuum, we investigated $RaHfO_3$ crystal and gathered more data regarding its physical characteristics. We conducted a thorough examination of the physical properties of $RaHfO_3$'s crystal structure, employing Perdew Burke Ernzerhof (PBE), Revised Perdew Burke Ernzerhof (RPBE), PBE sol, and B3LYP functionals to assess its geometric, electronic structure, mechanical, thermodynamic, and optical characteristics. This work promises to provide useful insights for future experimental investigations, particularly with the understanding of the underlying structure of materials and the interpretation of numerous phenomena within these fields.

2. Computational details

In this study, a 6 × 6 × 6 k-point mesh was employed, and pseudopotentials with a 500 eV cutoff energy were used to achieve high accuracy in the calculations [15]. Structural optimization was carried out using the BFGS algorithm, with total energy convergence achieved to within 0.2000×10^{-4} eV/atom. Additionally, the maximum ionic force was recorded as 0.5000×10^{-1} eV/Å, the maximum ionic displacement was 0.2000×10^{-2} Å, and the maximum stress component was 0.1000 GPa.

3. Results and discussion

3.1. Optimized structure analysis

The structural optimization of $RaHfO_3$ crystals was initiated with a lattice parameter of a = b = c = 3.780 Å and angles α = β = γ = 90°. The optimized $RaHfO_3$ crystal adopts a cubic structure with the space group $Pm\bar{3}m$ [221]. The associated point group for the crystal is Pm3m, and the Hall symbol for this crystal system is -P 423, providing additional crystallographic information. Table 1 provides an overview of the final optimized $RaHfO_3$ setups. and the cubic structure of the $RaHfO_3$ crystal is presented Figure 1.

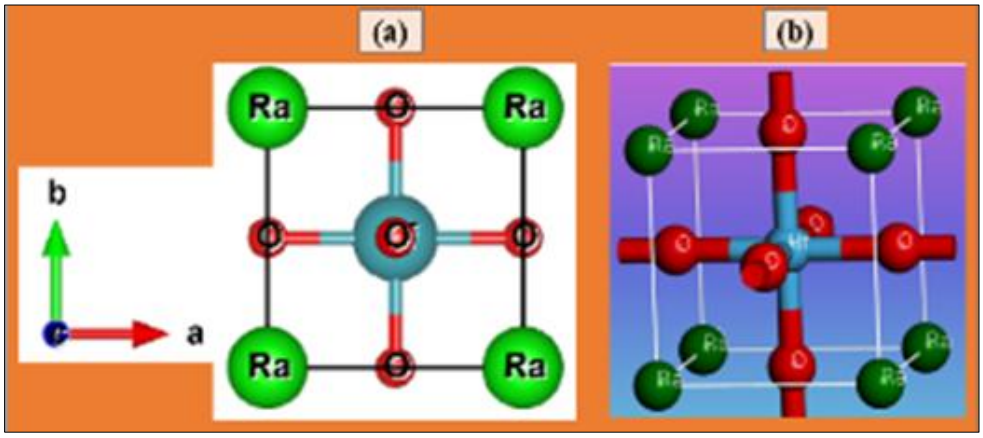

Figure 1 Crystal structure of RaHfO3 using (a) Vesta software (b) Castep mode

Table 1 Optimized lattice parameter, Cell volume and Final energy of $RaHfO_3$ crystal

Compound	Lattice parametera=b=c (Å)	Cell volume (Å^3)	Final Energy (eV)	Methods
$RaHfO_3$	4.076249	67.730174	-2056.837983781	PBE
	4.093945	68.616105	-2058.117738439	RPBE
	4.053073	66.581465	-2052.028824654	PBE sol
	3.780000	54.010152	-2050.889512034	B3LYP

3.2. Electronic band structure

Determining a material's electronic characteristics requires knowing its band structure, which offers crucial information about its energy levels and band gaps. Materials are classified as insulators, semiconductors, or metals based on their band structure, particularly the band gap energy [16-17]. Analysis of the $RaHfO_3$ crystal in Figure 2, reveals its semiconductor nature, determined by small band gap values calculated using methods like PBE, RPBE, PBEsol, and B3LYP. The study confirms an indirect band gap, with the conduction band minimum and valence band maximum at different k-points (X-R-M-Γ-R), as summarized in Table 2.

Table 2 Bandgap values of $RaHfO_3$ crystal

Compounds	Bandgap Value (eV)		Methods
$RaHfO_3$	2.247	PBE	
	2.178	RPBE	
	2.095	PBE sol	
	3.520	B3LYP	

The density of states (DOS) is presented to elucidate the distribution of electronic energy levels in a material as a function of energy [18-19]. A DOS plot clearly delineates occupied and unoccupied states, with metals often displaying a high DOS at the Fermi level. The total density of states (DOS) and partial density of states (PDOS) for $RaHfO_3$ are depicted in Figure 3, as computed using several densities functional theory (DFT) approaches. The semiconductor properties of $RaHfO_3$ are enhanced by the little difference noted between the electronicstates in the valence and conduction bands. The highest density of states values in the valence and conduction bands are around 6.0 electrons/eV and 5.10 electrons/eV, respectively.

The PDOS analysis Figure S1, (ESI) indicates that in the valence band, the Ra atom mostly contributes through the p orbital, the Hf atom through the s and d orbitals, and the O atom through the s orbital [20]. The predominant contributions in the conduction band originate from the Ra-d, Hf-d, and O-p orbitals. The significant peak in the conduction band results from the synergistic influence of Ra-s, Hf-d, and O-p orbitals, as examined by PBE, RPBE, PBEsol, and B3LYP methodologies. The valence band predominantly consists of Ra-s/p, Hf-d, and O-s/p orbitals.

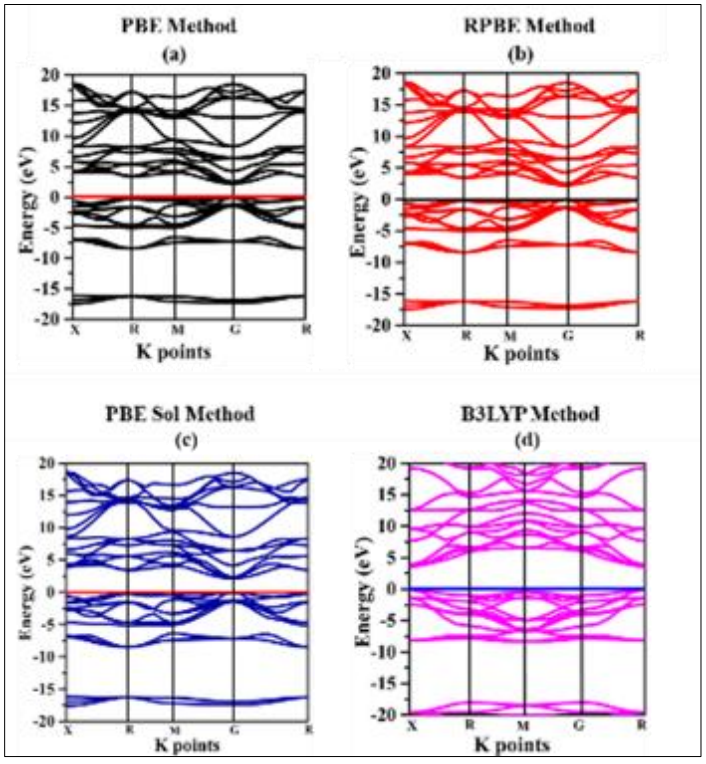

Figure 2 Band structure of $RaHfO_3$ by (a) PBE, (b) RPBE (c) PBEsol and (d) B3LYP methods respectively

The p orbital predominantly influences the valence band, providing around 5.2 electrons per electron-volt, whereas the d orbital substantially impacts the conduction band, with a contribution of around 4.10 electrons/eV. Furthermore, Mulliken atomic population analysis was part of a larger investigation of the crystals' bonding properties [21]. Oxygen exhibited a negative atomic charge, whereas radium and hafnium displayed positive charges. Furthermore, it was observed that the radium and hafnium atoms conveyed their electric charge to the oxygen atom. Table S1 (ESI) presents the bond length, population and charges of $RaHfO_3$ crystal.

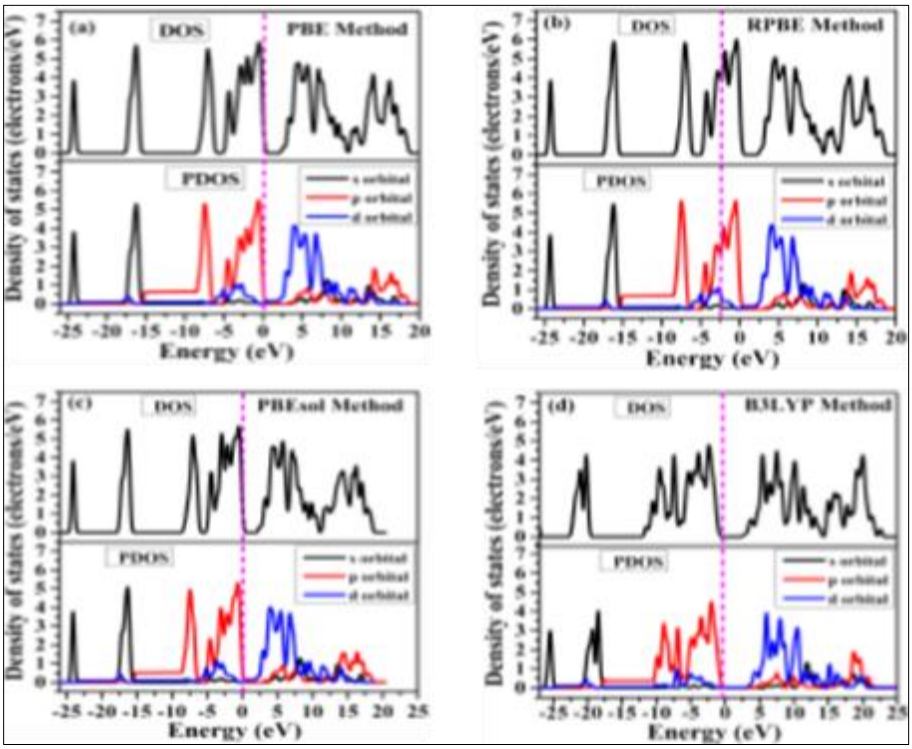

Figure 3 DOS and PDOS of $RaHfO_3$ crystal

3.3. Mechanical Properties

The mechanical stability of cubic $RaHfO_3$ is confirmed by the satisfaction of the Born stability conditions, which are provided as [22]: $C_{11} > 0$, $C_{44} > 0$, $C_{11} - C_{12} > 0$ and $C_{11} + 2C_{12} > 0$. Table 3 delineates the mechanical characteristics of $RaHfO_3$, computed by PBE, RPBE, and PBEsol, affirming its stability under certain circumstances. The Cauchy pressure, defined as $C_{12} - C_{44}$, offers insights into the material's response to stress-induced volume changes. Positive values observed for $RaHfO_3$ indicate metallic and ductile properties. Pugh's ratio (B/G), a metric for fragility or flexibility, was calculated as 1.25 (PBE), 0.75 (RPBE), and 0.57 (PBEsol), confirming ductile behavior. Consistency between Pugh's ratio and Cauchy pressure reinforces the validity of these results. High bulk modulus values indicate strong elasticity, incompressibility, and rigidity, enabling $RaHfO_3$. The shear modulus reflects strong resistance to shear deformation, ensuring structural stability [23]. Poisson's ratio values of 0.18, 0.19, and 0.20 (from PBE, RPBE, and PBEsol, respectively) indicate robust atomic and molecular interactions, while ratios closer to 0.5 suggest weaker bonding. The universal anisotropy index values of 0.33, 0.41, and 0.25 show moderate anisotropy, confirming the cubic $RaHfO_3$ crystal's high stiffness and mechanical stability [24].

Table 3 Elastic constants (Cij), Cauchy pressure (C12 – C44), bulk modulus (B), Young's modulus (Y), shear modulus (G), values (B/G), Poisson's ratio (v) and anisotropy factor (A)

Method Name	C_{11}	C_{12}	C_{44}	C_{12}- C_{44}	B	Y	G	B/G	v	A
PBE	321.46	83.43	40.04	43.04	133.85	252.23	106.34	1.25	0.18	0.33
RPBE	269.63	65.54	35.77	29.77	113.72	206.2	86.10	0.75	0.19	0.41
PBE sol	331.83	56.56	29.59	26.97	130.33	228.10	94.38	0.57	0.20	0.25

3.4. Thermo-physical features

The thermo-physical characteristics of $RaHfO_3$ crystals are presented in Figures 4 (a-e), offering insights into entropy, enthalpy, free energy, and heat capacity under varying conditions. Entropy reflects the level of disorder within a system and is directly proportional to the substance's quantity [25]. A systematically structured system demonstrates reduced entropy, as seen by the entropy of $RaHfO_3$ at 1000 K, computed to be 0.68 eV, 0.65 eV, and 1.0 eV utilizing the PBE, RPBE, and PBEsol methodologies, respectively, as illustrated in Figures 4(a), (b), and (c). These values suggest reduced molecular disturbances, indicating an ordered structure. Enthalpy, denoting the total thermal energy of a system and defining energy exchange with its environment in the absence of mechanical effort or heat transfer [26], demonstrated to rise with temperature in Figures 4(a), (b), and (c). The enthalpy values increase from 0.01 eV at 200 K to 0.20 eV, 0.23 eV, and 0.25 eV at 1000 K, as determined by the PBE, RPBE, and PBEsol techniques, respectively. This pattern signifies an augmentation in the system's thermal energy as the temperature rises.

Free energy, which quantifies the work a system can perform during thermodynamic processes [27], is shown in Figures 4(a), (b), and (c) to increase for $RaHfO_3$ from 0.02 eV at 180 K to 0.15, 0.17, and 0.19 eV at 1000 K using PBE, RPBE, and PBEsol methods, respectively. These variations highlight the crystal's dynamic response under changing thermal conditions. Heat capacity measures the thermal energy required to raise a material's temperature and reflects its ability to absorb or release energy under thermal fluctuations [28]. Materials with high heat capacities maintain stable thermal conditions, essential for various applications. Figures 4 (a), (b), and (c) illustrate the heat capacity of $RaHfO_3$, showing a peak at 1000 K with energy variations depending on the computational method (PBE, RPBE, and PBEsol). These results collectively underscore $RaHfO_3$'s thermo-physical stability, thermal resistance, and suitability for applications requiring robust energy absorption and dissipation properties.

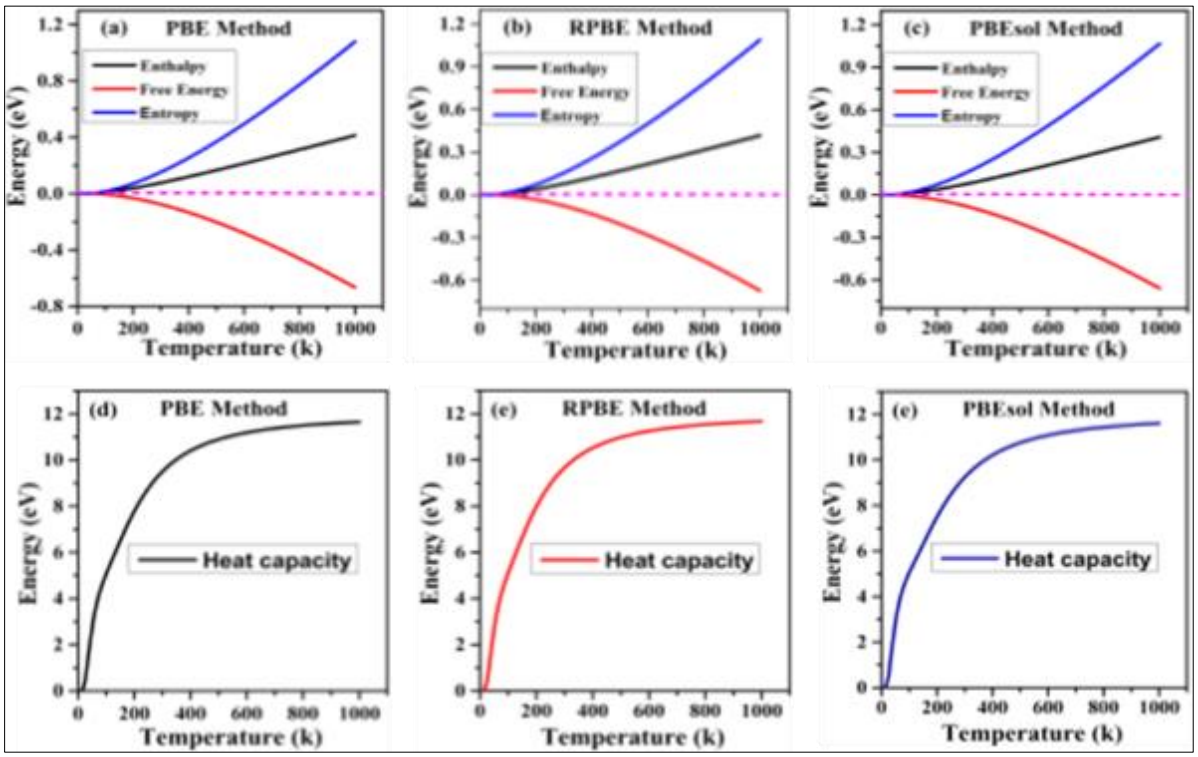

Figure 4 Enthalpy, Entropy, Free energy of $RaHfO_3$ in (a) PBE (b) RPBE (c) PBE sol methods respectively and (d), (e) and (f) Heat capacity in different method

3.5. Optical Properties

A Gaussian smearing of 0.1 eV was employed in all computational methods for the investigation of the optical properties of $RaHfO_3$. Reflection measurements shown in Figure 5, reveal a significant increase in reflectance from 1.0 eV to 23 eV, with all methods indicating reflectivity near 21.5 eV. The energy loss function, a critical parameter for optimizing energy efficiency in optoelectronics [29], is presented in Figure S2 (ESI). Results indicate that PBE and B3LYP methods yield lower energy loss [30] compared to RPBE and PBEsol, providing valuable guidance for selecting accurate computational approaches for $RaHfO_3$'s optical property predictions. Optical conductivity reflects a material's ability to transmit visible light, with the real component indicating conductivity and the imaginary component representing energy dissipation

[31]. As shown in Figure S3 (ESI), $RaHfO_3$'s real component surpasses the imaginary component between 2.5 and 10.0 eV, then gradually decreases by 25 eV. Conversely, the imaginary component dominates from 10.0 to 25.0 eV, highlighting variations in energy absorption and conductivity.

Dielectric functions are crucial for understanding optical behavior and designing custom blends [32]. Figure S4 (ESI) shows that the real part of $RaHfO_3$ dominates over the imaginary part between 0 to 4.60 eV, then decreases towards 25.0 eV. Between 4.60 and 25.0 eV, the imaginary part exceeds the real part, indicating significant absorption under an electric field. Similarly, the refractive index analysis (Figure S5, ESI) reveals an inverse relationship between real and imaginary components across different methods [33]. $RaHfO_3$ exhibits greater absorption (imaginary part) than refraction (real part) from 2.5 to 25 eV, influencing its optical and absorptive properties for applications like filters and coatings.

The absorption spectra of $RaHfO_3$, as illustrated in Figure 6, are characterized by a consistent trend from 0 to 25 eV, as determined using the PBE, RPBE, PBEsol, and B3LYP techniques. Within the visible spectrum (1.78–4.14 eV or 300–700 nm), the material demonstrates significant absorption, with a peak occurring at 3.14 eV across all techniques employed [34-35]. Furthermore, the ultraviolet (UV) spectrum reveals numerous absorption peaks, with the most pronounced peak observed at 11.10 eV. This action highlights the remarkable and wide optical absorption characteristics of $RaHfO_3$ by demonstrating its efficiency in absorbing light in the visible and ultraviolet spectrums [36]. Furthermore, absorption coefficient curves of $RaHfO_3$ as a function of wavelength, are displayed in Figures 7 (a), (b), (c), and (d), respectively. Across the visible spectrum (300 to 700 nm), the figures show unique absorption peaks. The highest absorption for all four techniques was recorded around 350 nm. These wavelengths correspond to the regions where $RaHfO_3$ exhibits peak light absorption, highlighting its pronounced absorption properties at these specific wavelengths.

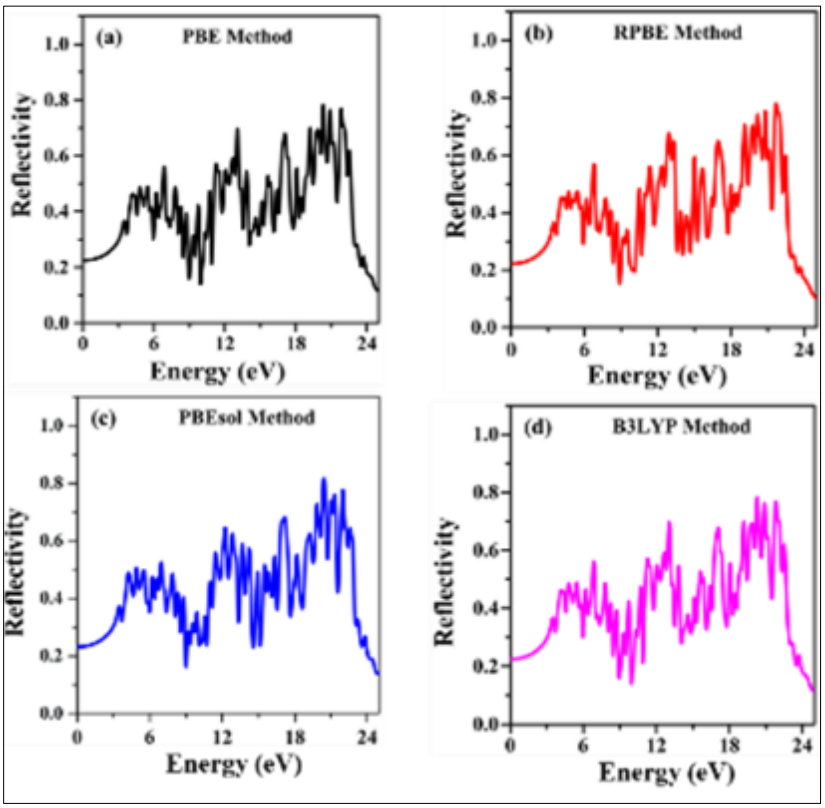

Figure 5 Optical Reflectivity of $RaHfO_3$ crystal (a) PBE (b)RPBE (c) PBE sol and (d) B3LYP methods

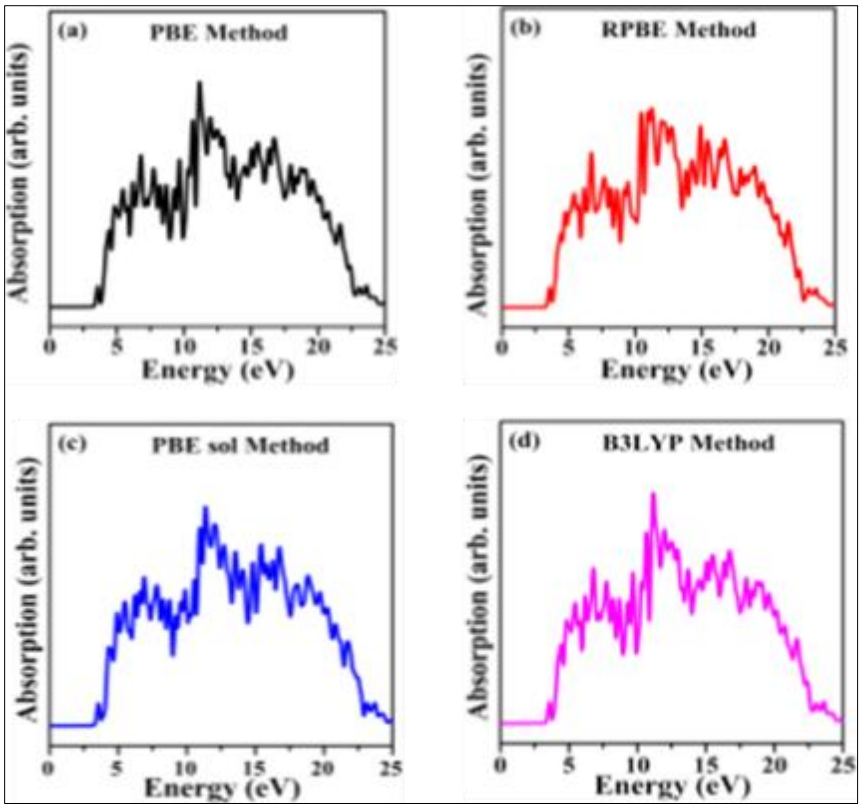

Figure 6 Optical absorption of $RaHfO_3$ crystal (a) PBE (b)RPBE (c) PBE sol and (d) B3LYP methods

Additionally, the absorption features in the visible range indicate that $RaHfO_3$ exhibits significant responsiveness to visible light, suggesting its potential for applications in optoelectronics and photocatalysis, where precise light manipulation and detection are crucial [37].

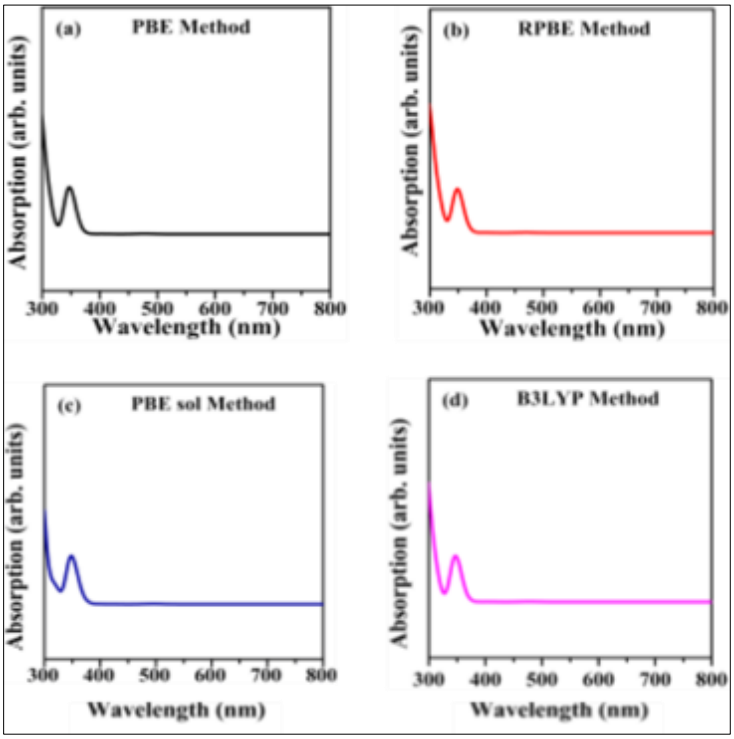

Figure 7 Absorption vs wavelength curve of $RaHfO_3$ crystal (a) PBE (b) RPBE (c) PBE sol and (d) B3LYP methods

4. Conclusion

The structural, mechanical, thermodynamic, and optical properties of $RaHfO_3$ have been comprehensively investigated using density functional theory (DFT). The calculated bandgap energies (Eg) reveal an indirect bandgap nature with values of 2.247 eV, 2.178 eV, 2.095 eV, and 3.520 eV, obtained using the PBE, RPBE, PBEsol, and B3LYP functionals, respectively. Mulliken population analysis has been employed to elucidate the bonding characteristics of $RaHfO_3$. The material exhibits remarkable mechanical and thermal stability, demonstrating significant ductility and elastic anisotropy, indicative of its resilience under mechanical stress. $RaHfO_3$ crystals might be exhibit exceptional photocatalytic properties due to their high absorption capacity across the visible and ultraviolet spectrum, as well as their narrow bandgap. This study highlights the potential of incorporating $RaHfO_3$ into a wide range of optoelectronic systems, contributing to advancements in the field of photocatalysts.

Compliance with ethical standards

Acknowledgments

The authors acknowledge the Department of Physics and ICT, European University of Bangladesh, Dhaka-1216, for providing facilities and support to carry out this work.

Disclosure of conflict of interest

The authors hereby declare there is no conflict of interest.

References

[1] Deng M, Shen S, Wang X, Zhang Y, Xu H, Zhang T, Wang Q. Controlled synthesis of $AgInS_2$ nanocrystals and their application in organic–inorganic hybrid photodetectors. CrystEngComm. 2013,15, 6443.

[2] Sen S k, Munshi M R, Kumar A, Mortuza A. A, Manir M S, Islam M A, Hossain M N, Hossain M K, Structural, optical, magnetic, and enhanced antibacterial properties of hydrothermally synthesized Sm-incorporating α-MoO_3 2D-layered nanoplates. RSC advances, 2022, 12,34584-34600.

[3] Liu Y, Zhang W, Wang B, Sun L, Li F, Xue Z, Nian H. Theoretical and experimental investigations on high temperature mechanical and thermal properties of $BaZrO_3$. Ceramic International, 2018, 44, 16475-16482.

[4] Feng, Zhenbao, Haiquan H, Shouxin C, Bai C. First-principles study of optical properties of $SrZrO_3$ in cubic phase. Solid State Communication, 2008, 148: 472-475.

[5] Islam M T, Kumar, A, Chakma U, Howlader, D. A computational investigation of electronic structure and optical properties of $AlCuO_2$ and $AlCu_{0.96}Fe_{0.04}O_2$: a first principal approach. Orbital: The Electronic Journal of Chemistry, 2021,13(1), 58-64.

[6] Amisi S, Bousquet E, Katcho K, Ghosez P. First-principles study of structural and vibrational properties of $SrZrO_3$. Physical Review B, 2012, 85, 064112.

[7] Kang S G, Sholl D S. First-principles investigation of chemical stability and proton conductivity of M-doped $BaZrO_3$ (M= K, Rb, and Cs). Journal of American Ceramic Society, 2017, 100, 2997-3003.

[8] Liu Q J, Liu Z T, Feng L P, Tian H. Mechanical, electronic, chemical bonding and optical properties of cubic $BaHfO_3$: First-principles calculations, Physica B, 2010 ,405, 4032–4039.

[9] Akther S, Abbas, S M E, Abbas S M G, Arshad M I. Batool J, Amin N. First-principles evaluation of electronic and optical properties of (Mo, C) codoped $BaHfO_3$ for applications in photocatalysis, Journal of Applied Physics. 2018, 123, 161569.

[10] Hoat D M, Silva J F R, Blas A M. First principles study of structural, electronic and optical properties of perovskites $CaZrO_3$ and $CaHfO_3$ in cubic phase, Solid State Communication, 2018,275, 29–34.

[11] Ahmed S, Zulfiqar W, Javed F, Arshad H, Abbas G, Laref A, Abbas S M A. Accurate first principles evaluation of structural, electronic, optical and photocatalytic properties of $BaHfO_3$ and $SrHfO_3$ perovskites, Journal of Alloys Compound, 2021, 892, 162071.

[12] Khenata R, Sahnoun M, Baltache H, Rérat M, Rashek A H, Illes N, Bouhafs B. First-principle calculations of structural, electronic and optical properties of $BaTiO_3$ and $BaZrO_3$ under hydrostatic pressure. Solid State Communication., 2005, 136, 120-125.

[13] Adewale A A, Chik A, Adam T, Yusuff O K, Ayinde S A, Sanusi Y K. First principles calculations of structural, electronic, mechanical and thermoelectric properties of cubic $ATiO_3$ (A= Be, Mg, Ca, Sr and Ba) perovskite oxide. Computational Condense Matter, 2021, 28, e00562.

[14] Muscat J, Wander A, Harrison N M. On the prediction of band gaps from hybrid functional theory. Chemical Physics Letter, 2001, 342, 397–401.

[15] Rizwan M, Aleena S, Shakil M, Mahmood T, Zafar A A, Hussain T, Farooq M H. A computational insight of electronic and optical properties of Cd-doped $BaZrO_3$. Chineese journal of Physics, 2020, 66, 318-326.

[16] Zahan M S, Munshi M R, Rana M Z, Masud M A. Theoretical insights on geometrical, mechanical, electronic, thermodynamic and photocatalytic characteristics of $RaTiO_3$ compound: A DFT investigation. Computational Condense Matter, 2023, 1, 36: e00832.

[17] Munshi M R, Masud M A, Khatun A. Structural, electronic, mechanical, thermodynamic and optical properties of oxide perovskite $BeZrO_3$: a DFT study, Physica Scripta, 2024, 99 (8), 085904.

[18] Munshi M R, Rana M Z, Sen S K, Foisal M R A, Ali M H. Theoretical investigation of structural, electronic, optical and thermoelectric properties of $GaAgO_2$ based on Density Functional Theory (DFT): Two approach. World Journal of Advance Research and Review, 2022, 13, 279–291.

[19] Haoui A, Elchikh M, Hiadsi S. Mechanical, optoelectronic and thermoelectric properties of the transition metal oxide perovskites $YScO_3$ and $LaScO_3$: first principle calculation, Physica B: Condensed Matter, 2023, 654, 414732.

[20] Munshi M R, Sen S K, Rana M Z. Electronic, thermodynamic, optical and photocatalytic properties of $GaAgO_2$ and $AlAgO_2$ compounds scrutinized via a systemic hybrid DFT, Computational Condense Matter, 2023 , 34, e00778.

[21] Rana M Z , Munshi M R , Masud M A, Zahan M S. Structural, electronic, optical and thermodynamic properties of $AlAuO_2$ and $AlAu_{0.94}Fe_{0.06}O_2$ compounds scrutinized by density functional theory (DFT). Heliyon, 2023, 9 ,11.

[22] Rahman N, Husain M,Yang J, Sajjad M, Murtaza G, Haq M U, Habib A, Zulfiqar, Rauf A, Karim A, Nisar M, Yaqoob M, Khan A. First principle study of structural, electronic, optical and mechanical properties of cubic fluoro-perovskites: ($CdXF_3$, X = Y, Bi). European Physical Journal Plus, 2021, 136, 347.

[23] Sohail M, Hussain M, Rahman N, Althubeiti K, Algethami M, Khan A A, Iqbal A, Ullah A, Khan A, Khan R. First-principal investigations of electronic, structural, elastic and optical properties of the fluoro perovskite $TlLF_3$ (L = Ca, Cd) compounds for optoelectronic applications. RSC Advances, 2022, 12, 7002-7008.

[24] Qaisi S A , Mebed A M , Mushtaq M , Rai D P , Alrebdi T A, Sheikh R A, Rached H , Ahmed R , Faizan M, Bouzgarrou S, Javed M A. A theoretical investigation of the lead-free double perovskites halides Rb_2XCl_6 (X= Se, Ti) for optoelectronic and thermoelectric applications. Journal of Computational Chemistry, 2023, 44(19), 690-1703.

[25] Kaufman L, Cohen M. Thermodynamics and kinetics of martensitic transformations. Progress in Physics of Metals, 1958, 7, 165–246.

[26] Rahman S, Hussain A, Noreen S, Bibi N, Arshad S, Rehman J U, Tahir M B. Structural, electronic, optical and mechanical properties of oxide-based perovskite ABO_3 (A = Cu, Nd and B = Sn, Sc): A DFT study. Journal of Solid State Chemistry, 2023, 317, 123650.

[27] Rehman J U, Usman M, Tahir M B, Hussain A , Rashid M. Investigation of Structural, Electronics, Optical, Mechanical and Thermodynamic Properties of YRu_2P_2 Compound for Superconducting Application. Journal of Superconductivity and Novel Magnetism, 2021, 34, 3089–3097.

[28] Colmenero F., Timón V., 2018 Study of the structural, vibrational and thermodynamic properties of natroxalate mineral using density functional theory. J. Solid State Chem. 263, 131–140.

[29] Ferrari A M, Orlando R, Rérat M. Ab Initio Calculation of the Ultraviolet–Visible (UV-vis) Absorption Spectrum, Electron-Loss Function, and Reflectivity of Solids. Journal of Chemical Theory and Computation, 2015,11, 3245–3258.

[30] Islam M A, Islam J, Islam M N, Sen S K, Hossain A K M A. Enhanced ductility and optoelectronic properties of environment-friendly $CsGeCl_3$ under pressure. AIP Advances, 2021, 11, 045014.

[31] Kora H H, Taha M, Abdelwahab A, Farghali A A, El-dek S I. Effect of pressure on the geometric, electronic structure, elastic, and optical properties of the normal spinel MgFe2O4 : a first-principles study. Materials Research Express, 2020, 7, 106101.

[32] Qaisi S A , Mushtaq M, Alzahrani J S, Alkhaldi H, Alrowaili Z A, Rached H, Haq B U, Mahmood Q, Buriahi M S A, Morsi M. First-principles calculations to investigate electronic, structural, optical, and thermoelectric properties of semiconducting double perovskite Ba2YBiO6. Micro and Nanostructures, 2022, 170, 207397.

[33] Dey A, Sharma R, Dar S A, Wani I H. Cubic PbGeO3 perovskite oxide: a compound with striking electronic, thermoelectric and optical properties, explored using DFT studies. Computational Condensed Matter, 2021, 26, e00532.

[34] Munshi M R, Zahan M S, Rana M Z, Masud M, A. First principles prediction of structural, electronic, mechanical, thermodynamic, optical and photocatalytic properties of In (X) O2, where X= Cu, Ag crystal scrutinized by density functional theory. Computational Condensed Matter, 2024, 38, e00884.

[35] Rahman S, Hussain A, Noreen S, Bibi N., Arshad S, Rehman J U, Tahir M B. Structural, electronic, optical and mechanical properties of oxide-based perovskite ABO3 (A= Cu, Nd and B= Sn, Sc): A DFT study. Journal of Solid State Chemistry, 2023, 317,123650.

[36] Munshi M R , Masud M A, Rahman M, Khatun M R, Mian M F. First principles prediction of geometrical, electronic, mechanical, thermodynamic, optical and photocatalytic properties of RaZrO3 scrutinized by DFT investigation, Computational Condensed Matter, 2024, 38.

[37] Babu K E, Veeraiah A, Swamy D T, Veeraiah V. First-principles study of electronic and optical properties of cubic perovskite CsSrF3, Material science Poland, 2012, 30, 359-67.